Aerospace Science and Technology 78 (2018) 271–279

Contents lists available at ScienceDirect

Aerospace Science and Technology

www.elsevier.com/locate/aescte

Three-dimensional through-flow modelling of axial flow compressor rotating stall and surge

Mauro Righi, Vassilios Pachidis, László Könözsy *, Lucas Pawsey

Cranfield University, Cranfield, Bedfordshire, MK43 0AL, United Kingdom

ARTICLE INFO

Article history:
Received 8 December 2017
Received in revised form 27 March 2018
Accepted 12 April 2018
Available online 17 April 2018

Keywords:
Post-stall modelling
Through-flow code
Rotating stall
Surge
Axial compressors
Godunov-type schemes

ABSTRACT

This paper presents a three-dimensional through-flow approach based on the cylindrical Euler equations incorporating a body force method. Blade performance is captured through a mixture of empirical correlations and a novel reverse flow treatment. The code is the first application of a physically correct Godunov solver to three-dimensional rotating stall and surge modelling. This solver ensures the accurate calculation of inter-cell fluxes unlike in typical modern CFD codes in which the non-linear convective terms are linearised. Validation consists of modelling a low speed three-stage axial compressor in all operating regions, recreating the reverse flow, rotating stall and forward flow characteristics with good agreement to experimental data. Additional comparisons are made against rotating stall cell size and speed, to which good agreement is also shown. The paper ends with some full surge cycle simulations modifying both the tank volume after the compressor and the level of inlet distortion applied. Both tank volume and level of distortion have been found to affect the type of instability developed. The development of this code is a step forward in compressor rotating stall and reverse flow modelling and allows recreation of a full compressor map at a significantly low computational cost when compared to commercially available 3D CFD codes.

© 2018 The Authors. Published by Elsevier Masson SAS. This is an open access article under the CC BY license (http://creativecommons.org/licenses/by/4.0/).

1. Introduction

The operation of a jet engine is limited by the onset of compressor stall. Rotating stall and surge are still not fully understood, neither in the mechanism through which the instability is triggered and subsequently develops, nor the aerodynamic load that is imposed on individual turbomachinery components during the event. This generally leads to a conservative approach during the design of blades and casings, and penalises the nominal operability range of the engine. Numerous solutions have been investigated to suppress the occurrence of compressor stall and increase surge margin. Experimental tests include axisymmetric arc-shaped slots casing treatment, investigated by Pan et al. [1], and bend skewed casing treatment tested by Alone et al. [2] Other recent methods proposed to increase the stability limit are recessed blade tips [3], casing grooves [4] and radial injectors [5]. Mhosen et al. [6] numerically investigated the use of tandem rotor blades to improve the flow turning and diffusion and suppress passage separation. Imani and Montazeri-Gh [7] proposed an improvement on the Min–Max limit protection in the control of aero-engines to reduce the possibility of accidental crossing of the stability limit. Aero-engines embedded in airframes are a common feature of next-generation aircrafts but the unsteady flow distortion generated by the S-ducts greatly reduce the surge margin. Gil-Prieto et al. [8], developed a method to predict peak levels of distortions in S-ducts in order to avoid extensive experimental testing and continuous redesign of the compressor when matching inlet duct and engine. The various post-stall behaviours that a multi-stage compressor can exhibit were demonstrated by Day and Freeman [9] on a Rolls-Royce VIPER compressor. As illustrated in Fig. 1, at high speeds the compressor is prone to surge, while at mid speed it forms a full span stall cell and at low speeds a front end stall.

Full characterisation of the post-stall behaviour of a high speed compressor experimentally is expensive. CFD modelling of axial turbomachinery in full 3D has been successfully achieved in the past, however the computational cost required is significant. In 1999 in a joint effort NASA and GE simulated the GE90 turbine system (18 blade rows) using 3D CFD [10]. The 9 million elements model was run on 121 processors in parallel and it took 15 hours to converge to a single operating point, in 10000 iterations. Gourdain et al. [11] simulated rotating stall using a quasi-3D code and modelling a stream surface; yet still a single stage of compression required 8 hours per revolution on a 32 core system. This reduced-order CFD was able to simulate a stable stall but the predicted

* Corresponding author.
E-mail address: laszlo.konozsy@cranfield.ac.uk (L. Könözsy).

https://doi.org/10.1016/j.ast.2018.04.021
1270-9638/© 2018 The Authors. Published by Elsevier Masson SAS. This is an open access article under the CC BY license (http://creativecommons.org/licenses/by/4.0/).

Nomenclature

B	Greitzer's parameter	–	
b	Blockage parameter	–	
f	Volumetric force	N/m^3	
W_{EX}	Work exchange	W/m^3	
E_0, H	Internal energy, Enthalpy	J/m^3	
E, F, G, S	Euler equations fluxes and source term		
M	Mach number	–	
P	Pressure	Pa	
R_{CUR}	Radius of curvature	m	
r	Radius	m	
T	Temperature	T	
t, τ	Time, time constant	s	
u	Air velocity	m/s	
U	Blade velocity	m/s	
U	Conservative variables		
x	Axial position	m	
α	Air flow angle	rad	
β	Camber-line direction	rad	
γ	Stagger angle	rad	
γ	Specific heat ratio	–	
δ	Deviation	rad	
θ	Circumferential position	rad	
ρ	Density	kg/m^3	
Ψ	Total-to-total pressure rise coefficient	–	
ϕ	Flow coefficient	–	
Ω	Rotational speed	rad/s	
ω	Pressure loss coefficient	–	

Subscripts

r, x, θ	Radial, axial, circumferential direction
η, ξ	Parallel, normal to camber-line direction
0	Total quantity
SS	Steady-state value

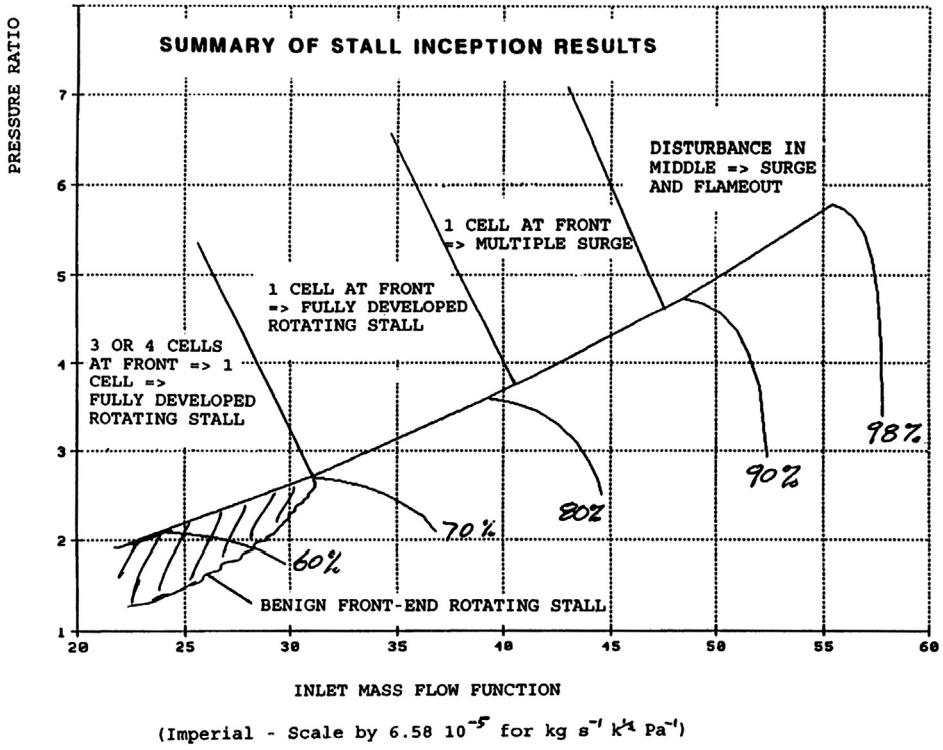

Fig. 1. Stall inception behaviour of Rolls-Royce VIPER compressor as simulated by Wilson [15].

number and speed of the cells was wrong. Khaleghi modelled rotating stall inception on a half annulus [12,13]. While the model had a span resolution at a low computational cost, this technique was able to simulate only modes multiple of two. More recently a URANS-based CFD method has been used to model stall in a modern high speed compressor by Dodds [14]. Modelling only the first three stages of the original eight, using the full annulus, one shaft revolution took 48 hours of computational time on 64 CPUs. An alternative to such an approach is the use of a through-flow code, which involves simplifying the problem using coarse grids and flow modelling based on the Euler equations with blade performance taken into account by empirical correlations. Such codes are extensively used in industry, with 2D codes looking only at the meridional plane and 3D codes modelling the full annulus, available for studying conventional pre-stall compressor performance. Some codes have been extended and adapted to simulate reverse flow and stalled flow, an example of which is Wilson [15] using a series of 1D through-flow codes in parallel to model the various stalling behaviours of the VIPER engine (as shown in Fig. 1). Gong [16] used a body force method, based on a database of correlations from conventional CFD, to model rotating stall. The tool was developed by a number of other researchers within MIT which improved the method, allowing it to be applied to a multi-stage axial compressor, as reported by Brand [17]. Longley [18] proposed a novel method to predict the region of highly separated flow which occurs during compressor stall. Since the circumferential element density is not enough to capture the separated flow between blade rows, Longley introduced a variable b that captures the flow non-uniformity. An equation is added that permits the creation, transport and mixing of the non-uniformity that represents the physics

of the flow, allowing the pressure loss and deviation during reverse flow to be sufficiently captured.

In almost all modern CFD codes the non-linear convective terms are linearised during the solution process, losing some physical features of the flow physics. The present paper proposes the application of a physically true solver to the already established methods of using body forces coupled with empirical correlations to model the post-stall behaviour of an axial compressor. The flow is modelled using the 3D cylindrical Euler equations and solved using a Godunov type solver. The scheme used is first order in time and space. Although it introduces substantial numerical diffusion this is necessary to maintain the solution stable as there is no other source of viscosity, either modelled or artificial. As described by Ekaterinaris [19] higher order schemes offer higher accuracy and lower numerical diffusion while still remaining computational efficient. The present code can be upgraded in the future to a higher order accurate scheme by increasing the order of the interpolation; however because of the lower numerical diffusion it will be necessary to model the viscosity in the equations. The theory and subsequent application and validation against low speed experimental results are presented in this paper.

2. Methodology

The tool developed is a through-flow code which solves the Euler equations in the empty annulus, using the body force method to simulate the presence of the compressor blading based on empirical correlations.

Governing equations and solver. The governing equations are written in a cylindrical coordinate system for an unsteady, inviscid compressible flow, and the continuity, momentum (Euler equation) and energy equations can be described in a compact form as

$$\frac{\partial}{\partial t}U + \frac{1}{r}\frac{\partial}{\partial r}(rE) + \frac{1}{r}\frac{\partial}{\partial \theta}F + \frac{\partial}{\partial x}G = S, \tag{1}$$

where the scalar governing equations can be written in a matrix form as

$$\frac{\partial}{\partial t}\begin{bmatrix}\rho\\ \rho u_r\\ \rho u_\theta\\ \rho u_x\\ \rho E_0\end{bmatrix} = -\frac{1}{r}\frac{\partial}{\partial r}\begin{bmatrix}\rho r u_r\\ \rho r u_r^2\\ \rho r u_\theta u_r\\ \rho r u_x u_r\\ \rho r H_0 u_r\end{bmatrix} - \frac{1}{r}\frac{\partial}{\partial \theta}\begin{bmatrix}\rho u_\theta\\ \rho u_r u_\theta\\ \rho u_\theta^2 + P\\ \rho u_x u_\theta\\ \rho H_0 u_\theta\end{bmatrix} - \frac{\partial}{\partial x}\begin{bmatrix}\rho u_x\\ \rho u_r u_x\\ \rho u_\theta u_x\\ \rho u_x^2 + P\\ \rho H_0 u_x\end{bmatrix} + \begin{bmatrix}0\\ \frac{\rho u_\theta^2}{r} - \frac{\partial P}{\partial r}\\ -\frac{\rho u_\theta u_r}{r}\\ 0\\ 0\end{bmatrix}. \tag{2}$$

These model equations are solved transiently in the full annulus on a relatively coarse grid required to maintain acceptable computational requirements. The results are obtained by using $2 \sim 5 \times 10^5$ elements for a four-stage compressor. A structured mesh is generated, based only on the annulus geometry, requiring the number of elements in each geometric direction as an input. An example mesh is shown in Fig. 2.

During a compressor stall it is expected that the pressure and flow field discontinuities play an important role in the dynamics of the stall. It is therefore necessary that any solver used is able to robustly and accurately model discontinuities and high gradients in flow properties (ρ, u, T) typical of reverse flow while using a coarse mesh. Finite volume methods using classic fluxes would not be optimal as they are known to introduce diffusivity and numerical oscillations in such conditions [20]. The MacCormack scheme

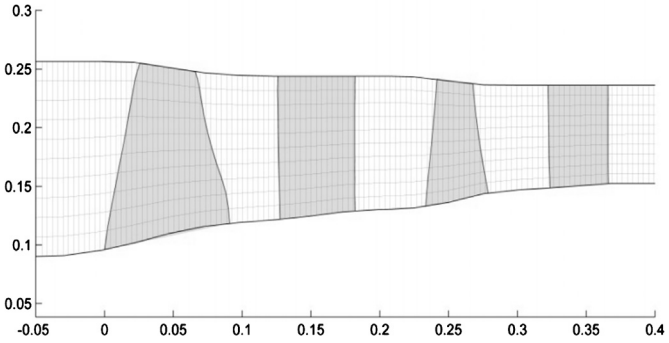

Fig. 2. Example grid generation for NASA TP1493 compressor rig [30].

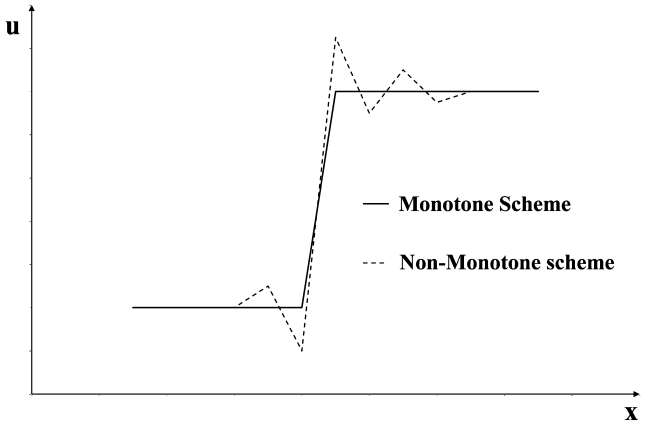

Fig. 3. Behaviour of monotone and non-monotone schemes in discontinuity modelling, based on original artwork by Hirsch [20].

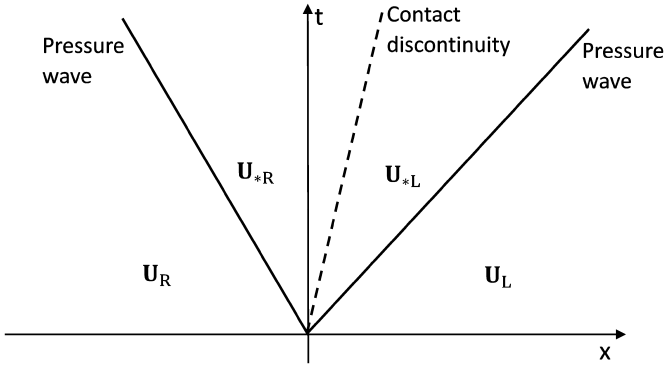

Fig. 4. Riemann problem solved at inter-cell boundaries.

(a shock capturing method [21]) was previously used within Cranfield in this same application to avoid diffusive errors but as a finite-difference method was prone to instability when high gradients occurred. In addition to this, artificial viscosity had to be introduced in order to stabilise the flow, which in turn was in conflict with the high gradients of the body force method and introduced significant numerical errors. To properly predict shocks on coarse grids monotonicity preserving (monotone or TVD, Total Variation Diminishing) schemes are considered appropriate as they do not introduce any spurious oscillations, with typical behaviour depicted in Fig. 3.

The Godunov scheme is a first-order, monotone, finite volume method which calculates the inter-volume fluxes based on states at the volume boundaries, obtained by solving the local Riemann problem [22].

The Riemann problem, shown in Fig. 4, is solved by modelling the wave amplitudes and the state between them, allowing the

physically correct upwinded fluxes to be calculated. As a monotone scheme the Godunov method guarantees to model accurately discontinuities and to avoid any unphysical behaviour (such as rarefaction shocks). As a first-order method the Godunov scheme introduces substantial diffusivity. However, it is suggested that it could be advantageous when simulating a compressor with the Euler equations to introduce some artificial diffusivity. Since shear stress is absent, the presence of some numerical viscosity would prevent unphysical solutions with extreme recirculation from arising. The scheme is applied in 3D as an unsplit finite volume method, which means that no dimensional splitting is used and the solution is advanced in time using all fluxes in a single step. The HLLC (Harten-Lax-van Leer-Contact) Riemann solver is used to model the waves at the boundaries [22]. Time stepping is performed by employing an explicit Forward Euler scheme, where the CFL condition can be expressed as

$$\Delta t \leq \frac{\Delta x}{2a_{max}}. \tag{3}$$

The Euler equations are modified inside of the blade rows by the following steps:

1. Adding a vector f containing the forces' source term.
2. Removing the fluxes in the tangential direction as these are not allowed in the presence of blades.
3. Introduce a term, as suggested by Gong [16], which translates the flow inside of the rotors with movement of the blades.

The equations inside the passage then become those shown in Equations (4)–(5), where Ω is zero for stator blades. The translational term is solved using a 3^{RD} order upwind scheme. Using this formulation allows to solve the whole domain, both static and rotating parts, in the absolute frame of reference.

$$\frac{\partial}{\partial t}U + \frac{1}{r}\frac{\partial}{\partial r}(rE) + \frac{\Omega}{r}\frac{\partial}{\partial \theta}U + \frac{\partial}{\partial x}G = S + f, \tag{4}$$

$$f = \begin{bmatrix} 0 \\ fr \\ f_\theta \\ f_x \\ W_{EX} \end{bmatrix}. \tag{5}$$

Body force method. To simulate the presence of the blades the body force method is used. As suggested by Longley [18] the length-scale of a rotating stall cell is greater than a few blade pitches, and it is then sufficient to model only a reduced number of virtual passages in place of the physical ones. The virtual passages are the tangential elements of the grid, with the number of elements in the order of the number of real blades. There is then no resolution of the flow profile inside the channels, instead the flow inside each grid element is a pitchwise average of the flow inside one channel or more. Since the number of virtual passages is constant along the compressor, the ratio of real/virtual passages varies between compressor stages and can be greater or less than unity. This is demonstrated in Fig. 5.

The passages are two-dimensional as they have axial and radial resolution; even though the flow can be instantaneously misaligned with the passage direction, the tangential flux is set to zero. The body forces consist of two terms:

- A turning force f_N turns the flow in the direction imposed by the blade without changing the total pressure in the relative frame of reference.
- A pressure loss force f_{PL} imposes locally the total pressure loss estimated by the empirical correlation, ΔP_0.

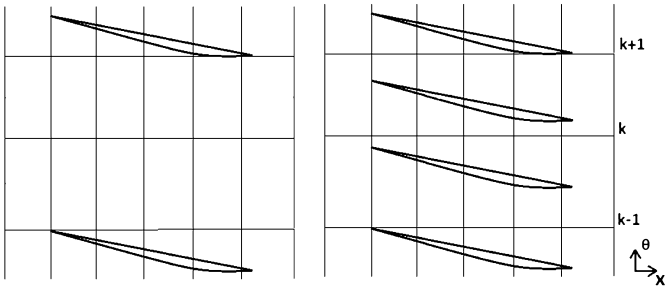

Fig. 5. Circumferential grid elements, with different real/virtual passages ratios between stages.

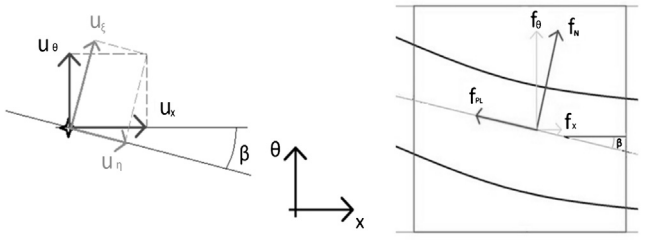

(a) Vectors along camberline direction (b) Body force composition

Fig. 6. Flow velocities and body force decomposition.

The body forces are calculated only along the planes formed by the grid; they are based on the velocity projection on the grid and applied back in the direction of the grid. Every component of velocity normal to them is not considered and is a source of error. The velocity along the plane is decomposed into a velocity parallel and normal to the camberline, u_η and u_ξ respectively. The projection of f_{PL} and f_N forms the three f forces in Equation (4). The work exchange term W_{EX} is calculated multiplying the force in the circumferential direction and the blade velocity (Fig. 6).

The direction which the body force imposes is based on the local camberline modified to match the inlet flow angle and the estimated deviation at the outlet, thus the virtual passage is always tangent to the incoming flow and the predicted outlet flow. The forces f_{PL} and f_N are projected in the instantaneous direction of the flow to avoid any interference of the turning and pressure loss effects. The forces are calculated based on the velocities in the relative frame of reference and then applied in the absolute frame. The body force formulations used, Equations (6)–(8), were derived from what was proposed by Longley [18] and Brand [17] as

$$f_{PL} = -\Delta P_0 \frac{P/P_0}{\Delta x \cdot \cos\beta}, \tag{6}$$

$$f_N = \frac{1 - M_x^2}{\cos^2(\beta)(1 - M^2)} \cdot \frac{\rho u_\eta^2}{R_{CUR}} + \frac{\tan\beta(1 + (\gamma - 1)M^2)}{1 - M^2} f_{PL} + f_{COR}, \tag{7}$$

$$f_{COR} = -\rho |u_x| \frac{u_\xi}{s \cdot \cos\beta} \cdot k. \tag{8}$$

The turning force consists of a main component, which takes into account the change in momentum along the local radius of curvature of the blade passage. This also includes the pressure gradient generated by the turning force itself and by the pressure loss force f_{PL}. The formulation is modified when M is near unity to avoid singularities.

The component f_{COR} is a corrective force which reacts to the misalignment between the direction imposed, β, and the actual flow direction; it is therefore proportional to the velocity component normal to the local imposed direction. This force is a function

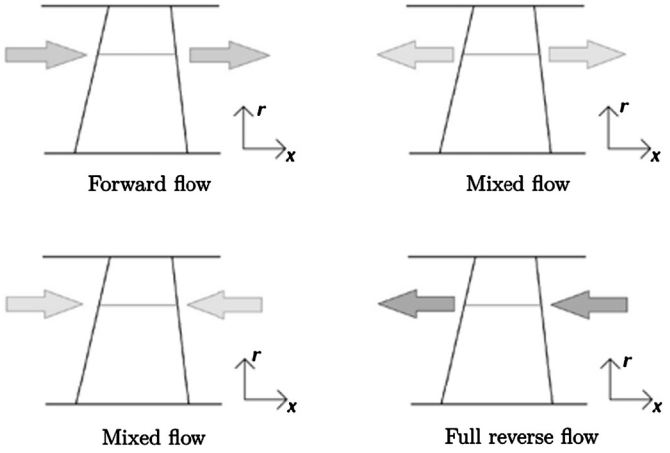

Fig. 7. Possible flow regimes.

of the blade pitch, however a constant k is necessary. The value of k is set large enough to ensure u_ξ is zero at the passage outflow in every regime; in the current case a value of 10 was found to be sufficient.

The total pressure loss across the blade row is calculated multiplying a pressure loss coefficient ω with the dynamic head at the inlet. The pressure loss is then distributed along the chord to obtain the pressure loss in every element ΔP_0; a sinusoidal distribution similar to that proposed by Gong [16] is used. The pressure loss coefficient ω and deviation δ are calculated using empirical correlations for every virtual blade passage at every grid plane. If the passage is unstalled then ω and δ are estimated using a set of correlations for forward flow reported by Aungier [23]. If it is stalled, then the correlation for separated passage flow, proposed by Thomason and Moses [24], is used.

To identify whether the blade passage is stalled, a criterion is used, proposed by Aungier [23] and based on the aerodynamic velocity ratio W_{RE}. The passage is stalled if

$$W_{RE} = \sqrt{\frac{P_{0\,OUT} - P_{OUT}}{P_{0\,IN} - P_{IN}}} < W_{MIN} \tag{9}$$

where W_{MIN} is the minimum velocity ratio before stall and is a function of the compressor geometry.

The empirical correlations used are valid only for steady flow. To account for the lag which occurs when the flow stalls or recovers the empirical coefficients are updated using a first-order time lag law, described in Eq. (10). The time constant τ is the time that the flow takes to cross the passage.

$$\partial\delta/\partial t = (\delta_{SS} - \delta)/\tau\ . \tag{10}$$

Reverse flow modelling. Flow modelling during stall requires the capability to deal with different regimes which appear as the flow reverses direction. These are identified at every time step, blade row, circumferential position and grid plane. They are grouped into three flow regimes: forward flow, fully reversed flow and mixed flow, Fig. 7.

The mixed flow regime is the most difficult to model as it requires more assumptions and uncertainty. Gamache [25] observed that inside a stall cell the flow is fully reversed whilst the mixed/inverting flow is present only in the thin boundary of the cell. It is then more important to accurately model the separated fully reversed flow as this has the greatest influence on the stalled performance.

The reversed regime is characterized by the separation of the flow inside and downstream of the blade. Models of separated flow

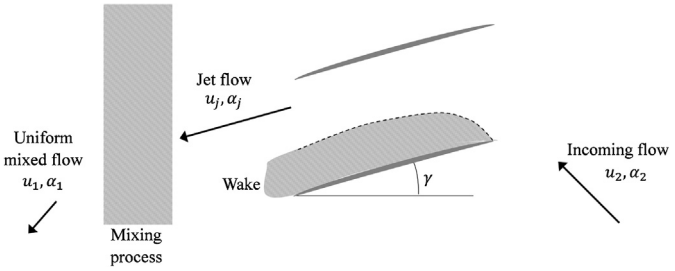

Fig. 8. Flow structure in a separated channel in reverse flow, based on the models by Longley [18] and Thomason and Moses [24].

have been developed by Thomason and Moses [24] and more recently by Longley [18], both based on similar assumptions:

- Flow separates on the suction surface and the mixing can continue after the trailing edge.
- The separated jet exits at the trailing edge with the direction of the stagger angle.
- Friction is negligible and the flow which forms the jet is isentropic, pressure loss derives from the separation.
- Deviation is due to the wake mixing.

In the model proposed by Longley the separation is produced by the force which abruptly turns the flow when it enters the blade at a high angle. This force is the integral of the pressure on the blade surface, and therefore it is always normal to the blade. As the force is directed against the incoming flow it introduces a pressure loss. The flow does not lose total pressure immediately but separates isentropically and the loss is not detectable until mixing occurs.

A similar approach is used in the current code. When mixed or reversed flow is present the imposed direction stops adapting to the incoming flow. The normal and parallel forces are replaced by only a turning force which is normal to the blade, and not aligned to the flow angle. The change in direction is provided by the correction force F_{COR} and ω is not calculated, the pressure loss is introduced naturally by the turning force directed against the flow. The deviation is imposed at the flow outlet (i.e. the leading edge) with the same method used for unstalled flow.

This system is preferred to the use of empirical correlations as it can be applied during mixed flow, when a clearly defined inlet or outlet does not exist and strong radial flow is present. The calculation of deviation has been developed starting from the model of Longley. The parameter b is defined in his model as the ratio between the real axial momentum of the separated flow and the axial momentum of the pitchwise averaged flow. It can be calculated from the inlet attack angle by using Eq. (11)

$$b = 1 + \left|\frac{\sin(\alpha_2 - \gamma)}{\cos(\alpha_2)}\right|. \tag{11}$$

By applying a control volume to the flow between states j and 1, as shown in Fig. 8, and by solving the momentum in the axial and tangential directions, the flow angle α_1 can be computed by Eq. (12), thus

$$\tan(\alpha_1) = \tan(\alpha_j) \cdot b. \tag{12}$$

However, whilst the model considers the flow in the passage to be fully isentropic, in reality the mixing occurs partly inside of the blade at the interface between the bubble and the jet. This is considered in the method of Longley through an entropy-generation term, which in every element where separation is present, mixes out the flow at a prescribed ratio. The prescribed ratio is such

as the excess energy, which is the energy contained in the non-uniformity of the flow, is mixed in the time taken for the jet to travel the distance of half a pitch.

In the formulation proposed by this author the equation modelling the b parameter is not used, therefore it is necessary to introduce the mixing directly in the deviation correlation. The point at which the full separation is reached is set at a quarter of the chord and from this point the profile of b in the passage is modelled based on a mixing ratio similar to that which was proposed by Longley. In the current case the distance used to set the mixing is not half the pitch, but twice the pitch; this was found to give appropriate results on a range of speeds on two different low-speed test cases. We can then estimate the value of b at the trailing edge, from which the angle post-mixing can be calculated. The deviation angle is then a function also of the blade solidity as

$$\delta = f(\alpha_{IN}, \gamma, \sigma). \tag{13}$$

As the deviation is calculated based on the inlet angle it cannot be estimated if the flow is exiting from both blade edges, in this case the flow exit angle is set as the metal outlet angle ($\delta = 0$).

Simulation method. The geometry input to the code consists of the annulus shape, the meridional position and shape of the blades, and the profiles along the span of inlet and outlet metal angles and stagger angle of each blade row. Additional details of the blade profiles are necessary depending on the forward flow correlation used.

Non-reflecting boundary conditions [26] are applied at inlet and outlet, applying total pressure and temperature where flow enters the domain and static pressure where flow exits the domain. With the current boundary conditions formulation, the flow entering the domain is assumed to be axial to the compressor. The presence of a combustor and turbine following the compressor is reproduced using a tank which discharges to the atmosphere through a nozzle, as is normal practice on an experimental compressor rig. This is simulated using a zero-dimensional model which models pressure and density based on the flux between the tank, the compressor outlet and the atmosphere. The volume of the tank is user-defined and influences the stall dynamics. The throttle can be changed dynamically as required during the simulation.

The simulation can be run with only a single tangential element, thus being axisymmetric; which is useful to quickly obtain a starting point for stall simulations, close to the surge margin. The simulation can then be loaded and restarted with a number of circumferential elements and the tank throttle model behind the compressor. The compressor is throttled to move the operating point beyond the stability line and the stall is allowed to develop. For the compressor to develop a physically correct rotating stall cell, some asymmetry must be introduced artificially. In this code asymmetric variations of pressure were introduced in the inlet flow field, which was found to be sufficient to produce (in the correct conditions) a rotating stall. Other methods to introduce asymmetry include introducing random disturbances into the flow field, as done by Longley [18], or changing slightly the geometry of the compressor to replicate manufacturing tolerances.

3. Results and discussion

Experimental results from a low speed 3-stage compressor, as reported by Gamache [25] and Eastland [27], were selected as a validation case. Two builds were tested by Gamache, all results presented here are for the moderate reaction build. Steady characteristics for reverse flow and rotating stall were obtained, as well as flow profiles and stall cell information. Maps were reported in the form of static-to-static, total-to-static and total-to-total pressure rise characteristics. In the following results the total-to-total ratio is used, ψ_{TT}.

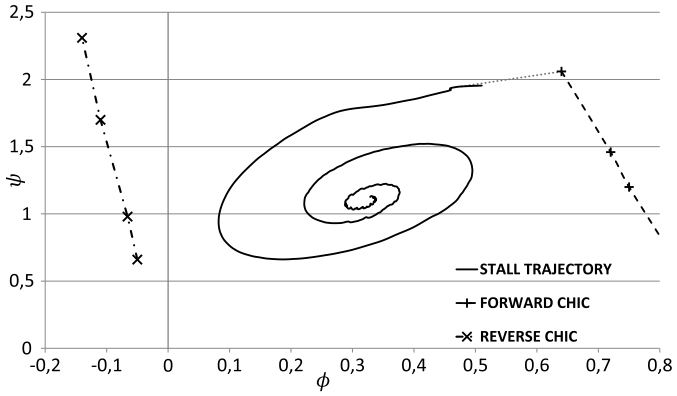

Fig. 9. Trajectory of rotating stall inception.

Full map creation. The full map consists of the forward and reverse flow characteristics, with the forward flow characteristics formed of a rotating stall and pre-stall characteristic. To obtain the reverse flow characteristic the code is run with a single element in the circumferential direction, thus modelling the flow as axisymmetric. Boundary conditions are fixed and the simulation is run to a converged state. To check for numerical or physical hysteresis, simulations were started with initial conditions of both reverse and forward unstalled flow, with identical results in each case. Experimental data is reported for three compressor speeds, 1170, 1800 and 2400 RPM, however on a map of flow coefficient ϕ against pressure rise coefficient ψ the characteristics collapse onto the same line. These are defined as

$$\phi = u_x/U\,, \tag{14}$$

$$\psi = \frac{P_{0\,OUTLET} - P_{0\,INLET}}{0.5\rho U^2}\,. \tag{15}$$

These definitions are based on velocity and density upstream of the IGV. The full reverse characteristic is obtained by changing the boundary conditions in steps and allowing a settling time. The time required for each simulation is in the region of thirty minutes. A comparison is made against the experimental results in Fig. 10, with the simulation matching the trend of the experimental rig, suggesting the formulation proposed for reverse flow is appropriate.

For rotating stall only the highest speed of 2400 RPM was modelled, with the grid containing 64 elements in the circumferential direction. Stall was obtained using the same methodology as previously described, starting from a simulation close to the stall line and reducing the throttle further whilst simultaneously introducing a distortion at the inlet. Again, two levels of distortion and throttle closure are carried out for the first point to ensure repeatability of results that are independent of the triggering mechanism. Subsequent points are obtained by incremental throttle changes. The simulation shown in Fig. 9 has a physical time of 500 ms (20 revolutions) and was obtained in approximately ten hours.

Successive movements on the map are obtained in physical times of up to 350 ms, depending on the flow coefficient. High flow coefficient points reach stability in longer times, suggesting that in this part of the map the characteristic is almost overlapping with the throttle characteristic and the stability is weak. The full map comparing all three regions to the experimental results is shown in Fig. 10. The forward flow region of the map is not reproduced with significant accuracy, however this characteristic

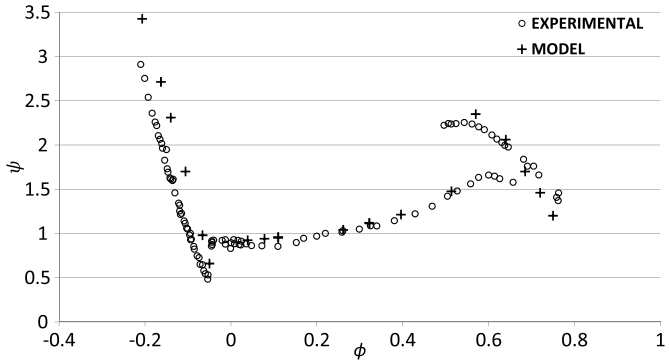

Fig. 10. Full compressor map comparing simulated and experimental performance.

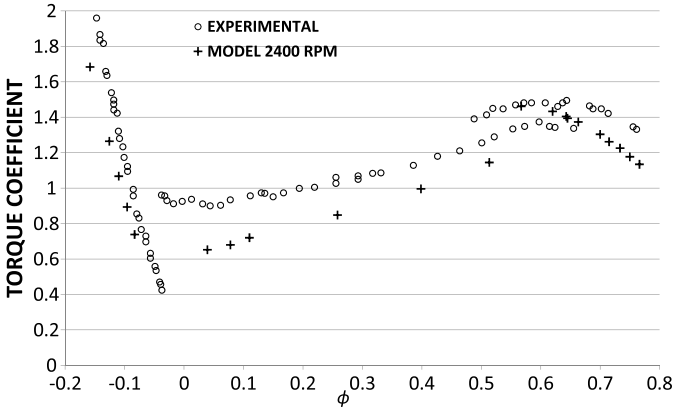

Fig. 11. Full torque compressor map comparing simulated and experimental performance.

depends heavily on the correlations used, which in this case are taken from open literature and clearly do not represent accurately this compressor. The matching of the forward flow characteristic was not pursued further, as it was outside of the research scope. In the operating conditions reported by Eastland choking never occurs, and therefore the code capability of capturing the correct choking massflow was not addressed. Overall the map has been recreated with a good matching.

There is no data on the compressor efficiency, but the measured torque coefficients are available for all the regimes [27,25]. In steady state conditions the matching of the torque signifies the correct modelling of the total temperature rise, and thus of the efficiency. The results of the modelled and measured torque are compared in Fig. 11. The results from the simulations have a similar trend to the experimental characteristic but with a constant offset. Only at very low positive ϕ the trend of the results from the code diverges from the experimental ones.

Rotating stall cell properties. The model simulated a single rotating stall cell for all flow coefficients, in line with the experimental findings. The compressor rig was probed using a traverse hotwire in front of the IGV. During rotating stall the passage of the cell leaves a trace in the hotwire voltage, which can be used to determine the speed of the stall cell based on the period of the trace. The size can be inferred from the ratio of the distorted region of the trace on the overall period. Mimicking the post-processing technique described by Gamache on the simulation results, the rotating stall cell speed and size are compared against the experimental results in Figs. 12 and 13.

The simulated stall cell speed is lower than the measured speed but it captures correctly the range and trend, although the minimum was located at a higher flow coefficient. The trend also agrees with the experimental rule that part span stalls rotate faster than

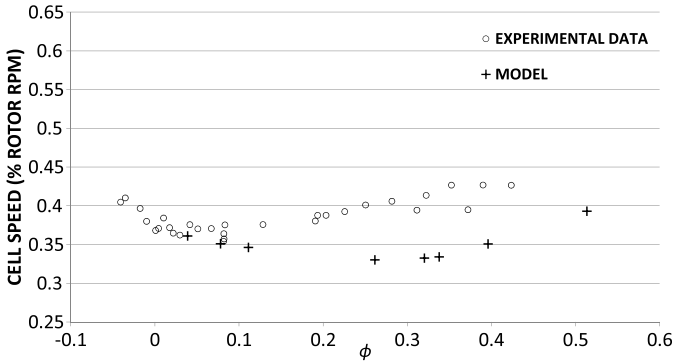

Fig. 12. Comparison of simulated stall cell speed at IGV inlet against experimental data.

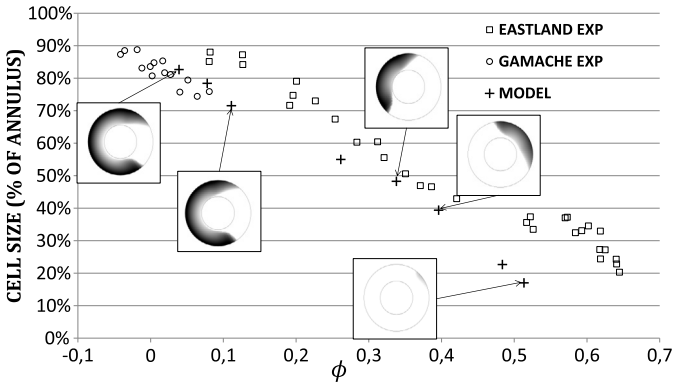

Fig. 13. Comparison of simulated stall cell size at IGV inlet against experimental data, overlaid with simulated contour of axial velocity showing reversed flow in black.

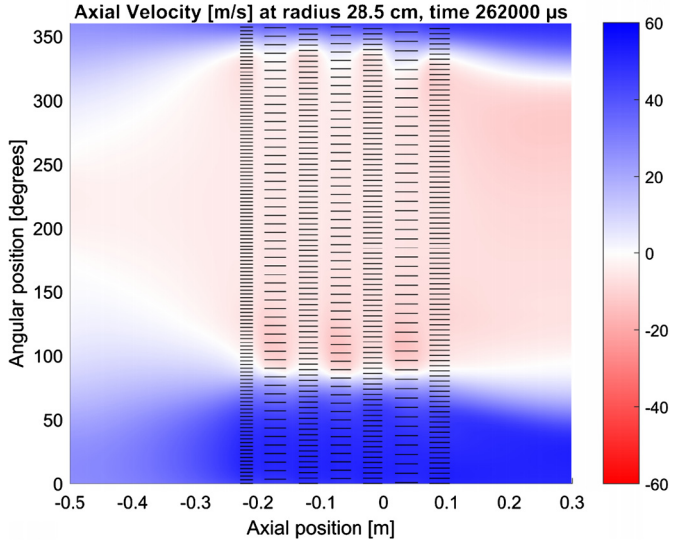

Fig. 14. Axial velocity at a constant radius, showing the shape of the stall cell across the compressor stages. (For interpretation of the colours in the figure(s), the reader is referred to the web version of this article.)

full span [28]. The size of the cell is more difficult to compare against due to the ambiguity of the experimental measurement, with data from the two sources, Gamache and Eastland, proving to be discontinuous as shown in Fig. 13. Despite this, the overall trend is correctly captured. An example of the cell shape across the compressor stages is shown in Fig. 14.

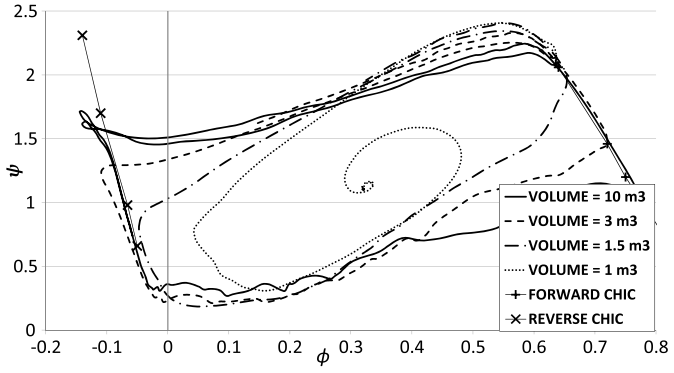

Fig. 15. Comparison of surge cycle simulations with different tank volumes.

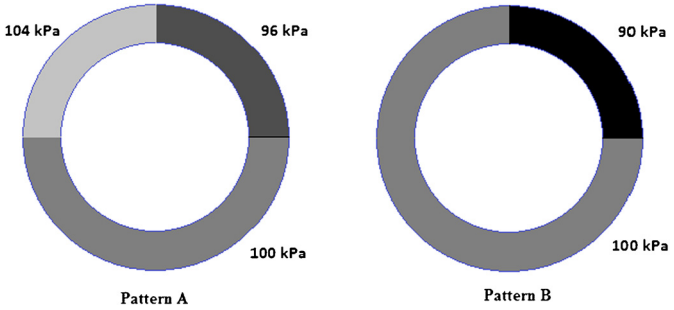

Fig. 16. Types of distortion of inlet total pressure used in stall simulations.

Surge simulation. Following the creation of a steady characteristic map, the model was used to simulate different types of surge cycle. The model, similar to that described previously to simulate rotating stall, has the inlet disturbance reduced with two 90° sectors of −4 kPa and +4 kPa, relatively, lasting for 10 ms at the start of the simulation alongside each other. In this way, the asymmetry is not driving the event and it is only present in the background. Many simulations are run with differing volume sizes, using the same constant throttle setting and the same rotational speed of 2400 RPM. As seen in Fig. 15, the largest volume produces a deep surge cycle with little overshoot that follows closely the steady characteristic with an almost constant pressure ratio during the reversal and recovery phases of the cycle.

As the volume reduces the behaviour becomes more dynamic, including larger overshoots on the blowdown phase and a cycle that is more oblique in shape, reflecting what Day found experimentally [29]. Once the volume is small enough, in this case 1 m^3, the flow does not fully reverse and during the recovery phase it develops a mature locked-in rotating stall, finding equilibrium on the rotating stall characteristic.

The cases which surged never developed a strong asymmetric flow pattern. This pattern grows during the blowdown and re-pressurisation phase of the cycle; while the compressor is operating in fully reverse flow instead it reduces, and when following the unstalled forward flow characteristic it is removed completely. As the case with 1 m^3 volume never reaches the reverse flow characteristic the asymmetry continues to grow and in this particular scenario the compressor is not able to recover.

To further verify the capability of the code to predict the correct outcome of a stall event a further simulation is carried out using the same conditions as in the 3 m^3 volume case. As described in literature [28] with the same RPM, throttle, tank volume, the system has the same Greitzer parameter, B. The same initial conditions are exposed to a more aggressive pressure distortion at the inlet, −10 kPa on a 90° sector for 10 ms, this distortion is shown in Fig. 16 as Pattern B and compared to the distortion used previously for surge (pattern A).

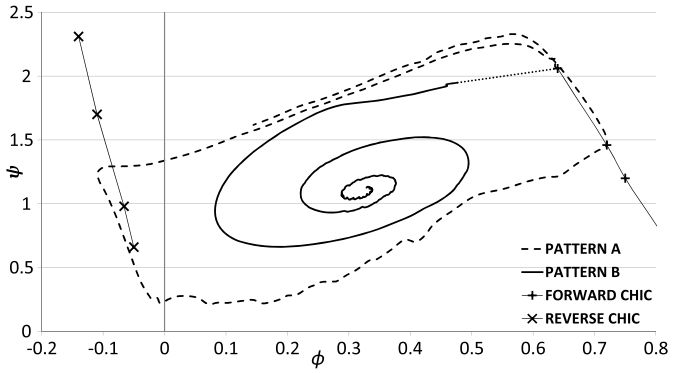

Fig. 17. Comparison of two events at same B parameter triggered using different inlet distortions.

Pattern B distortion guarantees that a rotating stall cell is formed immediately and as a result the operating point spirals down onto the characteristic line, as shown in Fig. 17. According to literature there should exist a value of the B parameter that characterises when the compressor transitions from a surge cycle to locked-in rotating stall, which was shown with the previous simulations to occur between a volume of 1 and 1.5 m^3. This current simulation lies far outside this boundary yet still manages to lock-in stall, demonstrating the dependence on the triggering mechanism of the stall and not just global performance parameters. In this regard, the developed code proves useful as it is able to predict the outcome of two different stall triggering mechanisms.

Validation of the surge cycle was not possible since the compressor was not tested under these conditions. Surge cycles at different B parameters were modelled and reported by Gamache, however these are also a function of the throttle capacity which is not reported, hence a comparison is not possible.

4. Conclusions

A 3D tool capable of simulating rotating stall and surge was developed based on the Godunov finite volume solver, the body force method and empirical correlations. This work is the first application of a Godunov type solver to rotating stall and surge modelling, the features of this scheme are deemed particularly beneficial for this application. A new formulation for treating reverse flow has been proposed, a simplified method based on the blockage/non-uniformity model. The new tool was tested on a low-speed three stage compressor with the following outcome:

1. The steady reverse characteristic has been reproduced for different rotational speeds, exhibiting good agreement with the experiment data and enforcing the applicability of the developed simplified reverse flow model.
2. Rotating stall was simulated obtaining a very good agreement with the entire measured characteristic. The accuracy of the simulated performance is enhanced through comparisons of the stall cell speed and size with experimental values.
3. Deep surge was simulated for different system volumes in agreement with the expected behaviour, with validation not possible due to lack of experimental data. Through changing the distortion level the dependence of the stall outcome was demonstrated, allowing different behaviours for the same Greitzer parameter.

The validation carried out demonstrates the applicability of the proposed formulation to low-speed compressors, with successful simulation of all three operating regimes of the compressor. The developed tool is capable of reproducing the full compressor map

of a low-speed compressor in less than 72 hours, a computational cost unrivalled by modern 3D classical CFD codes.

Conflict of interest statement

None declared.

Acknowledgements

The authors would like to express their gratitude to Rolls-Royce plc. for funding this research and for permission to publish the paper. Special thanks to Mr. Arthur Rowe and Mr. Richard Tunstall from Rolls-Royce plc for supervising this work.

References

[1] T. Pan, Q. Li, Y. Wei, H. Lu, Effects of axisymmetric arc-shaped slot casing treatment on partial surge initiated instability in a transonic axial flow compressor, Aerosp. Sci. Technol. 69 (2017) 257–268, https://doi.org/10.1016/j.ast.2017.05.036.

[2] D.B. Alone, S.S. Kumar, M. Shobhavathy, J.R.R. Mudipalli, A. Pradeep, S. Ramamurthy, V.S. Iyengar, Experimental assessment on effect of lower porosities of bend skewed casing treatment on the performance of high speed compressor stage with tip critical rotor characteristics, Aerosp. Sci. Technol. 60 (2017) 193–202, https://doi.org/10.1016/j.ast.2016.11.006.

[3] Y.-J. Jung, H. Jeon, Y. Jung, K.-J. Lee, M. Choi, Effects of recessed blade tips on stall margin in a transonic axial compressor, Aerosp. Sci. Technol. 54 (2016) 41–48, https://doi.org/10.1016/j.ast.2016.04.009.

[4] J.-H. Kim, K.-J. Choi, K.-Y. Kim, Aerodynamic analysis and optimization of a transonic axial compressor with casing grooves to improve operating stability, Aerosp. Sci. Technol. 29 (1) (2013) 81–91, https://doi.org/10.1016/j.ast.2013.01.010.

[5] H. Khaleghi, Parametric study of injector radial penetration on stalling characteristics of a transonic fan, Aerosp. Sci. Technol. 66 (2017) 112–118, https://doi.org/10.1016/j.ast.2017.02.020.

[6] M. Mohsen, F.M. Owis, A.A. Hashim, The impact of tandem rotor blades on the performance of transonic axial compressors, Aerosp. Sci. Technol. 67 (2017) 237–248, https://doi.org/10.1016/j.ast.2017.04.019.

[7] A. Imani, M. Montazeri-Gh, Improvement of Min–Max limit protection in aircraft engine control: an LMI approach, Aerosp. Sci. Technol. 68 (2017) 214–222, https://doi.org/10.1016/j.ast.2017.05.017.

[8] D. Gil-Prieto, D.G. MacManus, P.K. Zachos, A. Bautista, Assessment methods for unsteady flow distortion in aero-engine intakes, Aerosp. Sci. Technol. 72 (Supplement C) (2018) 292–304, https://doi.org/10.1016/j.ast.2017.10.029.

[9] I. Day, C. Freeman, The unstable behaviour of low and high speed compressors, J. Turbomach. 116 (1994) 194–201, https://doi.org/10.1115/1.2928353.

[10] M.G. Turner, P.H. Vitt, D.A. Topp, S. Saeidi, S.D. Hunter, L.D. Dailey, T.A. Beach, Multistage Simulations of the GE90 Turbine, Tech. Rep. CR-1999-209311, NASA, 1999.

[11] N. Gourdain, S. Burguburu, F. Leboeuf, H. Miton, Numerical simulation of rotating stall in a subsonic compressor, Aerosp. Sci. Technol. 10 (1) (2006) 9–18, https://doi.org/10.1016/j.ast.2005.07.006.

[12] H. Khaleghi, Stall inception and control in a transonic fan, part a: rotating stall inception, Aerosp. Sci. Technol. 41 (2015) 250–258, https://doi.org/10.1016/j.ast.2014.12.004.

[13] H. Khaleghi, Stall inception and control in a transonic fan, part b: stall control by discrete endwall injection, Aerosp. Sci. Technol. 41 (2015) 151–157, https://doi.org/10.1016/j.ast.2014.12.022.

[14] J. Dodds, M. Vahdati, Rotating stall observations in a high speed compressor—part ii: numerical study, J. Turbomach. 137 (5) (2015), https://doi.org/10.1115/1.4028558.

[15] A.G. Wilson, Stall and Surge in Axial Flow Compressors, Ph.D. thesis, Cranfield University, 1996.

[16] Y. Gong, A Computational Model for Rotating Stall and Inlet Distortions in Multistage Compressors, Ph.D. thesis, Massachusetts Institute of Technology, 1999.

[17] M.L. Brand, An Improved Blade Passage Model for Estimating Off-Design Axial Compressor Performance, Ph.D. thesis, Massachusetts Institute of Technology, 2013.

[18] J.P. Longley, Calculating stall and surge transients, in: Proceedings of the ASME Turbo Expo, 2007.

[19] J.A. Ekaterinaris, High-order accurate, low numerical diffusion methods for aerodynamics, Prog. Aerosp. Sci. 41 (3) (2005) 192–300, https://doi.org/10.1016/j.paerosci.2005.03.003.

[20] C. Hirsch, Numerical Computation of Internal and External Flows: The Fundamentals of Computational Fluid Dynamics, Butterworth–Heinemann, 2007.

[21] R. MacCormack, The effect of viscosity in hypervelocity impact cratering, J. Spacecr. Rockets 40 (5) (2003) 757–763, https://doi.org/10.2514/2.6901.

[22] E.F. Toro, Riemann Solvers and Numerical Methods for Fluid Dynamics: A Practical Introduction, Springer Science & Business Media, 2013.

[23] R. Aungier, S. Farokhi, Axial-Flow Compressors: A Strategy for Aerodynamic Design and Analysis, Wiley, 2004.

[24] H. Moses, S. Thomason, An approximation for fully stalled cascades, J. Propuls. Power 2 (2) (1986) 188–189, https://doi.org/10.2514/3.22865.

[25] R.N. Gamache, Axial Compressor Reversed Flow Performance, Ph.D. thesis, Massachusetts Institute of Technology, 1985.

[26] T.J. Poinsot, S. Lelef, Boundary conditions for direct simulations of compressible viscous flows, J. Comput. Phys. 101 (1) (1992) 104–129, https://doi.org/10.1016/0021-9991(92)90046-2.

[27] A.H.J. Eastland, An Experimental Investigation of Compressor Performance in Rotating Stall, Ph.D. thesis, Massachusetts Institute of Technology, 1982.

[28] I. Day, Stall, surge, and 75 years of research, J. Turbomach. 138 (1) (2016), https://doi.org/10.1115/1.4031473.

[29] I. Day, Axial compressor performance during surge, J. Propuls. Power 10 (3) (1994) 329–336, https://doi.org/10.2514/3.23760.

[30] D.C. Urasek, W.T. Gorrell, W.S. Cunnan, Performance of Two-Stage Fan Having Low-Aspect-Ratio First-Stage Rotor Blading, Tech. Rep. 1493, NASA, 1979.

Cranfield University

CERES https://dspace.lib.cranfield.ac.uk

School of Aerospace, Transport and Manufacturing (SATM) Staff publications (SATM)

2018-04-17

Three-dimensional through-flow modelling of axial flow compressor rotating stall and surge

Righi, Mauro

Elsevier

Righi M, Pachidis V, Könözsy L, Pawsey L. (2018) Three-dimensional through-flow modelling of axial flow compressor rotating stall and surge, Aerospace Science and Technology, Volume 78, July 2018, pp. 271-279

https://doi.org/10.1016/j.ast.2018.04.021

Downloaded from Cranfield Library Services E-Repository